

Probing exotic cross-shell interactions at $N = 28$ with single-neutron transfer on ^{47}K

C. J. Paxman,¹ A. Matta,² W. N. Catford,¹ G. Lotay,¹ M. Assié,³ E. Clément,⁴ A. Lemasson,⁴ D. Ramos,⁴ N. A. Orr,² F. Galtarossa,³ V. Girard-Alcindor,⁴ J. Dudouet,⁵ N. L. Achouri,² D. Ackermann,⁴ D. Barrientos,⁶ D. Beaumel,³ P. Bednarczyk,⁷ G. Benzoni,⁸ A. Bracco,^{8,9} L. Canete,¹ B. Cederwall,¹⁰ M. Ciemala,⁷ P. Delahaye,⁴ D. T. Doherty,¹ C. Domingo-Pardo,¹¹ B. Fernández-Domínguez,¹² D. Fernández,¹² F. Flavigny,² C. Fougères,⁴ G. de France,⁴ S. Franchoo,³ A. Gadea,¹¹ J. Gibelin,² V. González,¹³ A. Gottardo,¹⁴ N. Goyal,⁴ F. Hammache,³ L. J. Harkness-Brennan,¹⁵ D. S. Harrouz,³ B. Jacquot,⁴ D. S. Judson,¹⁵ A. Jungclaus,¹⁶ A. Kaşkaş,¹⁷ W. Korten,¹⁸ M. Labiche,¹⁹ L. Lalanne,^{3,4} C. Lenain,² S. Leoni,^{8,9} J. Ljungvall,³ J. Lois-Fuentes,¹² T. Lokotko,² A. Lopez-Martens,³ A. Maj,⁷ F. M. Marqués,² I. Martel,²⁰ R. Menegazzo,²¹ D. Mengoni,^{21,22} B. Million,⁸ J. Nyberg,²³ R. M. Pérez-Vidal,^{11,14} L. Plagnol,² Zs. Podolyák,¹ A. Pullia,^{8,9} B. Quintana,²⁴ D. Regueira-Castro,¹² P. Reiter,²⁵ M. Rejmund,⁴ K. Rezynkina,^{26,21} E. Sanchis,¹³ M. Şenyiğit,¹⁷ N. de Séréville,³ M. Siciliano,^{14,18,27} D. Sohler,²⁸ O. Stezowski,⁵ J.-C. Thomas,⁴ A. Utepov,⁴ J. J. Valiente-Dobón,¹⁴ D. Verney,³ and M. Zielińska¹⁸

¹*School of Maths and Physics, University of Surrey, Guildford, GU2 7XH, United Kingdom*

²*Université de Caen Normandie, ENSICAEN, CNRS/IN2P3, LPC Caen UMR6534, F-14000 Caen, France*

³*Université Paris-Saclay, CNRS/IN2P3, IJCLab, 91405 Orsay, France*

⁴*Grand Accélérateur National d'Ions Lourds (GANIL), CEA/DRF-CNRS/IN2P3, Bvd Henri Becquerel, 14076 Caen, France*

⁵*Université Claude Bernard Lyon 1, CNRS/IN2P3, IP2I Lyon, UMR 5822, F-69100 Villeurbanne, France*

⁶*CERN, CH-1211 Geneva 23 (Switzerland)*

⁷*The Henryk Niewodniczański Institute of Nuclear Physics, Polish Academy of Sciences, ul. Radzikowskiego 152, 31-342 Kraków, Poland*

⁸*INFN Sezione di Milano, I-20133 Milano, Italy*

⁹*Dipartimento di Fisica, Università di Milano, I-20133 Milano, Italy*

¹⁰*Department of Physics, KTH Royal Institute of Technology, SE-10691 Stockholm, Sweden*

¹¹*Instituto de Física Corpuscular, CSIC-Universidad de Valencia, E-46101 Valencia, Spain*

¹²*IGFAE and Dpt. de Física de Partículas, Univ. of Santiago de Compostela, E-15758, Santiago de Compostela, Spain*

¹³*Departamento de Ingeniería Electrónica, Universitat de Valencia, Burjassot, Valencia, Spain*

¹⁴*Laboratori Nazionali di Legnaro, INFN, I-35020 Legnaro (PD), Italy*

¹⁵*Oliver Lodge Laboratory, The University of Liverpool, Liverpool, L69 7ZE, UK*

¹⁶*Instituto de Estructura de la Materia, CSIC, Madrid, E-28006 Madrid, Spain*

¹⁷*Department of Physics, Faculty of Science, Ankara University, 06100 Besevler - Ankara, Turkey*

¹⁸*Irfu, CEA, Université Paris-Saclay, F-91191 Gif-sur-Yvette, France*

¹⁹*STFC Daresbury Laboratory, Daresbury, Warrington, WA4 4AD, UK*

²⁰*Departamento de Ciencias Integradas, Universidad de Huelva, Calle Dr. Cantero Cuadrado, 6, 21004 Huelva, Spain*

²¹*INFN Sezione di Padova, I-35131 Padova, Italy*

²²*Dipartimento di Fisica e Astronomia dell'Università di Padova, I-35131 Padova, Italy*

²³*Department of Physics and Astronomy, Uppsala University, SE-75120 Uppsala, Sweden*

²⁴*Laboratorio de Radiaciones Ionizantes, Departamento de Física Fundamental, Universidad de Salamanca, E-37008 Salamanca, Spain*

²⁵*Institut für Kernphysik, Universität zu Köln, Zùlpicher Str. 77, D-50937 Köln, Germany*

²⁶*Université de Strasbourg, CNRS, IPHC UMR 7178, F-67000 Strasbourg, France*

²⁷*Physics Division, Argonne National Laboratory, Lemont (IL), United States*

²⁸*Institute for Nuclear Research, Atomki, 4001 Debrecen, P.O. Box 51, Hungary*

(Dated: September 20, 2024)

We present the first measurement of the $^{47}\text{K}(d, p\gamma)^{48}\text{K}$ transfer reaction, performed in inverse kinematics using a reaccelerated beam of ^{47}K . The level scheme of ^{48}K has been greatly extended with nine new bound excited states identified and spectroscopic factors deduced. Detailed comparisons with SDPF-U and SDPF-MU shell-model calculations reveal a number of discrepancies with these results, and a preference for SDPF-MU is found. Intriguingly, an apparent systematic overestimation of spectroscopic factors and a poor reproduction of the energies for 1^- states suggests that the mixing between the $\pi s_{1/2}d_{3/2}$ and $\pi s_{1/2}d_{3/2}$ proton configurations in ^{48}K is not correctly described using current interactions, challenging our descriptions of light $N = 28$ nuclei.

The nuclear shell model has long been established as the central theoretical approach to studying the structure of nuclei across the chart of isotopes [1–4]. At its core

is the premise that complex many-body nuclear systems may be described as protons and neutrons occupying orbitals of discrete energies, organized in shells. Specific

nuclear states are then obtained by computational diagonalizations of the nuclear Hamiltonian in a many-body model space consisting of one or more shells. This approach has been extremely effective in reproducing experimental observations, including excitation energies of nuclear states, spin-parity assignments, spectroscopic factors, and the emergence [5, 6] or weakening [7] of “magic numbers” (particularly stable configurations of nucleons). These models are partly phenomenological, and require experimental data to refine the interactions between orbitals. Hence, exotic cross-shell interactions – which are critical to the structure of exotic nuclear matter, but difficult to access experimentally – can be expected to be less well understood. There is significant need for experimental studies of the $\pi(sd)\text{-}\nu(fp)$ interactions, which will dominate the structure of neutron-rich nuclei from ^{42}Si to ^{60}Ca .

Previous studies of the $\pi(sd)\text{-}\nu(fp)$ interaction have been very successful, establishing the emergence of new magic numbers [5] and observing a critical weakening of p -wave spin-orbit splitting [8–10]. Of these, the interpretation of $^{46}\text{Ar}(d, p)$ is not straightforward due to the ground state structure of ^{46}Ar being poorly understood [11–13]. For the neighbouring ^{47}K nucleus, however, the ground state structure is well-understood due to a previous measurement of the magnetic moment [14]. Specifically, $^{47}\text{K}_{\text{g.s.}}$ has an unusual proton configuration, $\pi s_{1/2}d_{3/2}^4$, whereas its neighbour nuclei, $^{46}\text{K}_{\text{g.s.}}$ and $^{48}\text{K}_{\text{g.s.}}$, both have $\pi s_{1/2}d_{3/2}^3$ configurations [15]. This makes $^{47}\text{K}_{\text{g.s.}}$ a solid foundation for transfer reaction studies, whilst providing the first access to the $\pi(s_{1/2})\text{-}\nu(fp)$ interaction by this method.

The level structure of ^{48}K is largely unknown [16], and current shell-model calculations fail to reproduce the experimentally determined spin and parity (1^-) of the ground state. It seems that the mixing between the proton configurations $\pi s_{1/2}d_{3/2}^4$ and $\pi s_{1/2}d_{3/2}^3$, which coexist at near-degenerate energies, may play a key role in the structure of ^{48}K .

In this Letter, we present a detailed spectroscopic study of the nucleus ^{48}K , in which excited states up to and above the neutron-emission threshold energy ($S_n = 4.644$ MeV [18]) were populated via $^{47}\text{K}(d, p\gamma)$ transfer reaction in inverse kinematics. This selective reaction mechanism allows for the preferential population of single-particle levels in ^{48}K , thereby isolating states built upon the $\pi s_{1/2}d_{3/2}^4$ ground state of ^{47}K , with a neutron in the $\nu p_{3/2}$, $\nu p_{1/2}$, or hitherto-unexamined $\nu f_{5/2}$ orbitals. Moreover, in probing such states, this work represents a stringent test of modern shell-model calculations, requiring a need to account for both the neutron wavefunction and the mixing between the two proton configurations. In this regard, the unique combination [19] of the AGATA high-efficiency γ -ray tracking array [20, 21], the advanced MUGAST silicon array [22], and the VAMOS++ mag-

netic spectrometer [23], was of critical importance. In particular, it provided the background-free, ultra-high-resolution performance required to extract nuclear properties from excited states in odd-odd nucleus ^{48}K , which are closely spaced within the energy range $E_x = 0 - 4$ MeV.

A thick graphite target was bombarded with a 60 MeV/nucleon primary beam of ^{48}Ca , in order to produce a 7.7 MeV/nucleon beam of unstable ^{47}K ions, delivered by the SPIRAL1+ facility at GANIL [24]. This $>99.9\%$ pure secondary beam of ^{47}K , of intensity $\sim 5 \times 10^5$ pps, was directed onto a $0.31(2)$ mg/cm² thick self-supporting CD₂ target. Prompt γ rays were detected using the state-of-the-art AGATA tracking array [25–28], which in this instance consisted of 12 triple-cluster HPGe detectors mounted 18 cm from the target, covering angles $\theta_{\text{lab}} \sim 130 - 160^\circ$ [19]. Ejected protons were detected at backward angles ($\theta_{\text{lab}} \sim 104 - 156^\circ$) with the MUGAST double-sided silicon strip detector array, while beam-like heavy-ion recoils were transmitted to the focal plane of the VAMOS++ magnetic spectrometer (providing effective rejection of events resulting from reactions on carbon). Beam normalisation was achieved by monitoring incoming ^{47}K particles with a single CATS multiwire proportional counter [29] and by studying elastically scattered deuterons with a silicon detector, placed downstream of the target position. For proton energy calibrations, a triple- α source consisting of ^{239}Pu , ^{241}Am and ^{244}Cm was employed. The ^{48}K excitation energy (E_x) was reconstructed from the energy and the angle of the protons, requiring a coincidence with an ion at the VAMOS++ focal plane. Whilst the reconstructed excitation energy resolution was ~ 330 keV, the coincident γ -ray energy measurement allowed for a much higher effective resolution to be achieved. Gamma-ray energy and efficiency calibrations were carried out using a standard ^{152}Eu source, extrapolated to high energies through simulation [30]. Doppler correction of γ -ray energies was performed using velocities calculated event-by-event, from the observed proton energies and angles. The Doppler-corrected γ -rays had a resolution of 7 keV at 1.8 MeV, allowing for states that are unresolved in the particle-only spectrum to be separated in the particle- γ coincident spectrum, detailed below in Fig. 1.

An elastic scattering normalisation value, N_d (the product of the number of deuterons in the target and the integrated flux of the incoming beam), was determined by comparing elastically scattered deuteron data with optical model calculations. In this case, the optical model calculation was performed using the code FRESKO [31] and the potential of Daeknick, Childs and Vrcelj [32], although we note that DWUCK4 [33] produces entirely consistent results. Observed (d, p) proton events were reconstructed using the *nptool* framework [34], which also allowed a consistent efficiency determination using realistic GEANT4 Monte Carlo simulations [35]. The factor N_d

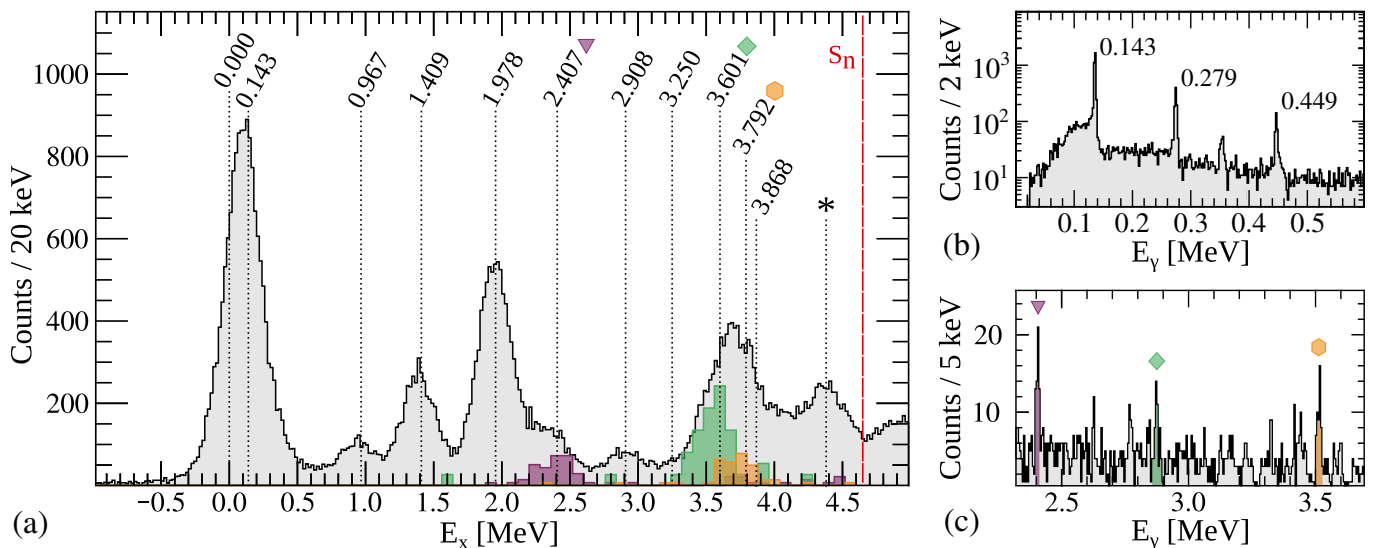


FIG. 1. (Color online) (a) Full reconstructed excitation energy spectrum of ^{48}K in black, with the neutron separation energy, $S_n = 4.644$ MeV, indicated. Peaks are labelled with their energies as determined by γ -ray spectroscopy. Three excitation energy spectra in coincidence with three observed γ -rays are shown in colour, showcasing how otherwise-unresolved peaks can be resolved. The peak marked with an asterisk represents an unresolved multiplet – see text. (b) Gamma-decays observed with AGATA over the energy range 0.0–0.6 MeV (cf. Table I). The small peak at 0.357(1) MeV corresponds to the decay of the first excited state in ^{47}K (slightly shifted due to its 1 ns lifetime [17]) which is populated here by the decay of neutron-unbound states in ^{48}K . (c) Gamma-decays observed with AGATA over the energy range 2.3–3.7 MeV. Symbols indicate the γ -rays (2.407, 2.872 and 3.516 MeV) used to construct the coloured excitation spectra.

was then applied to the observed angular distribution of these protons in order to obtain differential cross sections ($d\sigma/d\Omega$). For the extraction of spectroscopic factors, S , differential cross sections were compared with theoretical calculations determined from the code TWOFNR [36], using the Koning-Delaroche global optical potential [37] and Johnson-Tandy adiabatic model [38, 39]. In this analysis, the statistical error in extracting spectroscopic factors from differential cross sections is $<10\%$ [40]. However, the overall systematic uncertainty arising from reaction model limitations is expected to be $\sim 20\%$. This is illustrated in the analysis of Ref. [41], which also demonstrates that this technique, as discussed in Ref. [42], provides spectroscopic factors that can be compared directly to the shell model values. Shell model calculations were performed using the NuShellX code [43] to compute the first 40 states of each spin. Two state-of-the-art interactions were used, SDPF-U [44] and SDPF-MU [45, 46], as they are well-suited to describing nuclei in the region $N > 28$, $Z < 20$. Crucially, while the cross-shell $\pi(sd)\text{-}\nu(fp)$ component of the SDPF-U interaction is phenomenological in nature, in SDPF-MU this component is instead derived from first principles.

Table I presents the excitation energies, spin-parity assignments and spectroscopic factors of states in ^{48}K observed in this work, together with a comparison to current shell-model calculations, while Fig. 1 displays the excitation energy spectrum and coincident γ -ray spectrum observed in this work. With the exception of states

up to 0.8 MeV [16], all other states in ^{48}K are reported here for the first time. It is important to note that all levels observed in this study must have some wavefunction component of the unusual $\pi s_{1/2}d_{3/2}^4$ structure – we do not observe the three states above 0.8 MeV found by Królás *et al.* [16], as they have a structure based on the $\pi s_{1/2}d_{3/2}^3$ configuration.

In considering Fig. 1, several states in ^{48}K , such as the ground state and the first excited state (0.143 MeV), are unresolved. However, using the excitation energies obtained via γ -ray spectroscopy, a function was constructed which fit every state simultaneously, reproducing the excitation energy spectra well, across all angles. Hence, individual angular distributions were extracted for each state. Fig. 2 presents the $d\sigma/d\Omega$ of observed states, alongside theoretical calculations for $\ell = 1, 3$ transfer. As shown in Figs. 2(a) and (b), both the ground and first excited states in ^{48}K are well described by $\ell = 1$ transfer, in agreement with the previous 1_1^- and 2_1^- assignments [16]. Beyond the two lowest energy states, four strong peaks are observed in Fig. 1 at 0.967, 1.409, 1.978 and 2.407 MeV, respectively. An angular distribution analysis of these peaks, shown in Figs. 2(c)–(f), reveals pure $\ell = 1$ characters, indicating spin-parity assignments of 0^- , 1^- or 2^- . In comparison with shell-model calculations for p -wave states over the excitation energy range 0.5 – 3.0 MeV, we find that the properties of the presently observed 0.967, 1.409, 1.978 and 2.407 MeV levels follow the predicted ordering and γ -decay pathways

TABLE I. Properties of states observed in ^{48}K . Excited state energies were determined using γ -ray transitions observed from states populated directly in (d,p) or in cascade decays. Associated branching ratios (BR) are listed. Experimental spectroscopic factors S_{exp} are shown in comparison with shell-model calculations using the SDPF-MU [45, 46] (S_{MU}) and SDPF-U [44] (S_{U}) interactions. Upper limits on S_{exp} have been established from the non-observation of proton peaks.

E_x [MeV]	J^π	E_γ [MeV]	BR	$n\ell_j$	S_{exp}^a	S_{MU}	S_{U}
0.000	1^-	—	—	$2p_{3/2}$	0.24(5)	0.40	0.21
0.143(1)	2^-	0.143(1)	~ 100	$2p_{3/2}$	0.42(8)	0.86	0.84
0.279(1) ^b	2^-	0.279(1)	~ 100	$2p_{3/2}$	<0.03	0.01	0.05
0.728(3) ^b	3^-	0.449(2)	~ 100	$1f_{7/2}$	<0.04	0.06	0.05
0.967(2)	0^-	0.967(2)	~ 100	$2p_{1/2}$	0.26(5)	0.40	0.38
1.409(3)	1^-	1.130(3)	10(2)	$2p_{3/2}$	0.24(5)	0.35	0.54
		1.266(2)	63(2)				
		1.409(3)	28(1)				
1.978(4)	1^-	1.010(4)	5(1)	$2p_{1/2}$	0.50(10)	0.88	0.84
		1.836(3)	93(2)				
		1.979(3)	2(1)				
2.407(6)	0^-	0.997(4)	33(2)	$2p_{1/2}$	0.34(7)	0.56	0.58
		2.407(5)	67(7)				
2.908(8)	2^-	2.765(7)	~ 100	$2p_{3/2}$	0.023(5)	—	—
		—	—	$1f_{5/2}$	0.06(1)	—	—
3.250(6)	(3^-)	2.971(4)	~ 100	$1f_{5/2}$	0.06(1)	0.11	—
3.601(8)	2^-	2.193(3)	15(4)	$1f_{5/2}$	0.34(7)	0.47	0.50
		2.872(7)	38(7)				
		3.325(4)	22(5)				
		3.458(7)	12(4)				
		3.598(7)	12(4)				
3.792(8)	(3^-)	3.063(2)	12(4)	$1f_{5/2}$	0.16(3)	0.33	0.39
		3.516(7)	88(4)				
3.868(7)	(2^-)	3.727(6)	59(9)	$1f_{5/2}$	0.14(3)	0.18	0.21
		3.865(8)	41(9)				
		—	—				

^a Systematic uncertainty of 20% has been applied, see text.

^b State inferred from the γ decays of higher-energy excited states.

[40] of the 0_1^- , 1_2^- , 1_3^- and 0_2^- levels in ^{48}K , respectively. As such, we adopt these assignments here.

In contrast, at higher energies ($E_x > 3$ MeV) all states appear to be populated via pure f -wave ($\ell = 3$) transfer – see Figs. 2(h)-(i) – indicating J^π assignments of 2^- or 3^- , assuming transfer to the empty $f_{5/2}$ orbital. Of these, the 3.601 MeV state is the most strongly populated, with γ decays to 1^- , 2^- and 3^- levels. Both shell-model calculations predict that the state populated with the largest pure f -wave spectroscopic factor is a 2^- excited state. Therefore, we assign the 3.601 MeV state as 2^- . Additional, strong states at 3.792 and 3.868 MeV in ^{48}K are also found to be well reproduced by clear $\ell = 3$ transfers. The 3.792 MeV level is found to exhibit γ -ray transitions to 2^- and 3^- states, while the 3.868 MeV state decays to 1^- and 2^- states. In this light, we favour 3^- and 2^- assignments for these two states. In addition to the aforementioned 3.601, 3.792 and 3.868 MeV levels, a relatively weakly populated state at 3.250 MeV is found to decay via a 2.971 MeV γ ray to the second excited 2^- state. As

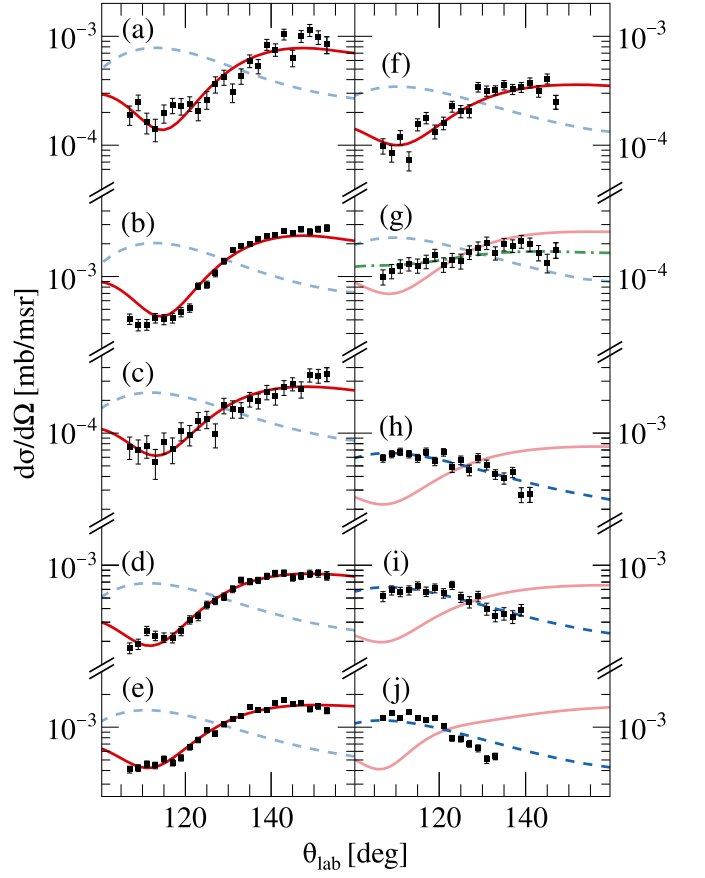


FIG. 2. Experimental differential cross sections for states observed in this work, with the scaled theoretical differential cross sections for $\ell_p=1$ ($\ell_p=3$) transfer in solid red (dashed blue) lines: (a) Ground state, (b) 0.143 MeV, (c) 0.967 MeV, (d) 1.409 MeV, (e) 1.978 MeV, (f) 2.407 MeV, (g) 2.908 MeV, (h) 3.601 MeV, (i) 3.792 & 3.868 MeV, (j) High energy multiplet. Only in the case of (g) was both $\ell=1$ and $\ell=3$ clearly required, with the best-fit shown in dot-dash green.

we do not observe the energetically favoured transition to the 1_1^- ground state, and based on reasonable matching to shell-model energies, we tentatively assign this state as 3^- .

Intriguingly, as can be seen in Fig. 2(g), we observe an excited state in the present data at 2.908 MeV that is not well reproduced by either a pure $\ell = 1$ or $\ell = 3$ distribution, and requires a mixed configuration, indicating a 2^- assignment. This is of particular significance as no such state is predicted by either shell-model calculation. Here, we extract $p_{3/2}$ and $f_{5/2}$ spectroscopic factors of 0.023(5) and 0.06(1) for the 2.908 MeV excited level. Furthermore, given this is the lowest-energy state to be observed in the current work to exhibit an f -wave component, we note that the presently observed 2.908 MeV excited state provides an excellent experimental marker for the location of the $f_{5/2}$ shell in this region of the nuclear chart.

We expect a number of levels to contribute to the peak labelled by an asterisk in Fig. 1. As such, an angular

distribution analysis was performed by considering this high-energy multiplet to be a single broad peak. Whilst pure $\ell = 3$ transfer reproduces the data well, as highlighted in Fig. 2(j), definitive spin-parity assignments could not be determined. Consequently, we simply report here an upper (lower) limit on the overall spectroscopic factor for this region ~ 4 MeV of 0.45 ± 0.09 (0.32 ± 0.07). Finally, for states above the neutron threshold, we attribute an integrated $\ell = 3$ spectroscopic factor of ~ 0.2 .

In evaluating the impact of the present work on nuclear structure around neutron number, $N = 28$, we first reiterate that these state-of-the-art shell-model calculations [43–46] fail to reproduce the 1^- ground state of ^{48}K , as shown in Fig. 3. This striking feature provides a key benchmark around $N = 28$ and emphasises the importance of theoretical improvements in this region, where the $\pi s_{1/2}$ and $\pi d_{3/2}$ orbitals are degenerate. Also clear in Fig. 3 is that the spacing between the pure $\ell = 1$ and pure $\ell = 3$ states (observed to be ~ 0.8 MeV) is overestimated by SDPF-U (~ 1.6 MeV), but closely reproduced

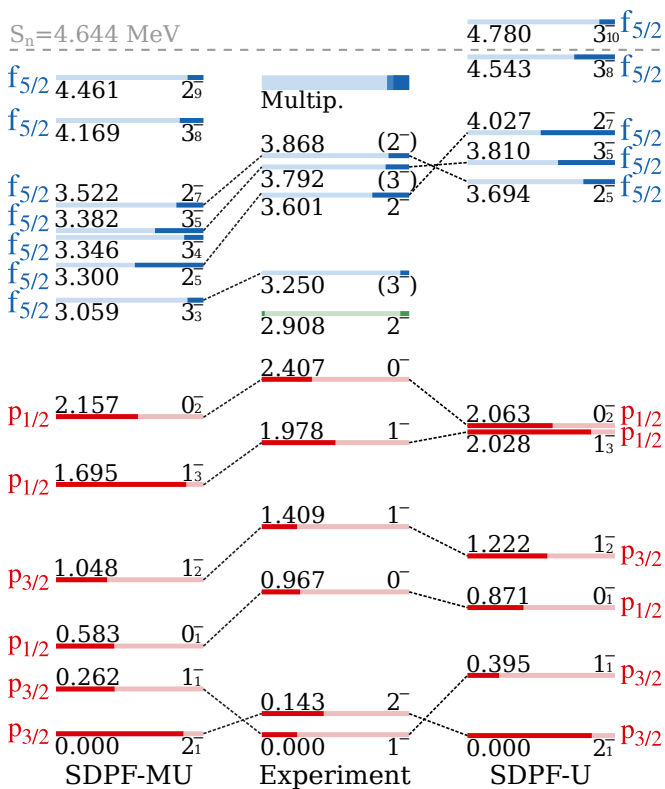


FIG. 3. Comparison of states directly populated by $^{47}\text{K}(d,p)$ as observed experimentally, and as predicted by shell model calculations using SDPF-MU [45, 46] and SDPF-U [44]. For each state, the filled length of the line represents the spectroscopic factor, S . All shell model states with $S \geq 0.1$ are shown. The p -wave (f -wave) states are shown in red (blue) and fill from the left (right). The mixed state (green) fills from both sides.

by SDPF-MU (~ 0.9 MeV). More quantitatively, the average energies of $\nu(p_{3/2})$, $\nu(p_{1/2})$ and $\nu(f_{5/2})$ – weighted according to S and $(2J+1)$ – are experimentally determined to be 0.45(2), 1.93(2) and 4.0(1) MeV, respectively [40]. This compares more favourably to SDPF-MU (0.56, 1.88 and 3.87 MeV) than SDPF-U (0.66, 2.12 and 4.35 MeV). Further, the splitting between the high and low spin projection of $\nu(p_{3/2})$, $\nu(p_{1/2})$ and $\nu(f_{5/2})$ are 0.42(2), 0.19(1) and < 0.8 MeV experimentally, again favouring SDPF-MU (0.76, 0.10 and 0.11 MeV) over SDPF-U (1.16, 0.44 and 0.24 MeV). Recall, however, that neither SDPF-MU nor SDPF-U shell-model calculations predict a neutron-mixed state with both p -wave and f -wave contributions, as observed in Fig. 2(g).

Interestingly, with the exception of the ground and first excited state in ^{48}K , the shell model correctly reproduces the ordering of observed $\ell = 1$ transfer levels. Furthermore, all excited states that are predicted to exhibit strong p -wave single particle strength by the shell model are observed experimentally here. However, experimentally deduced spectroscopic factors, S_{exp} , are considerably reduced relative to the proposed shell-model counterparts. Specifically, measured S_{exp} values are a factor ~ 0.5 – 0.7 lower than S_{MU} or S_{U} , as shown in Table I. This appears to be similarly true for $\ell = 3$ transfer, in spite of the fact that this analytical method should reproduce the shell model spectroscopic factors [41, 42].

An explanation for the observed discrepancies between theory and experiment may arise from the fact that states in ^{48}K with two different proton configurations coexist in the same energy regime. This is due to the near degeneracy of the $\pi s_{1/2} d_{3/2}^4$ configuration (as found in the ^{47}K ground state) and the $\pi s_{1/2}^2 d_{3/2}^3$ configuration. Assuming a single step process in the (d,p) reaction, states in ^{48}K are populated via the $\pi s_{1/2} d_{3/2}^4$ component of their wavefunction. In this regard, the shell model may not correctly predict the degree of mixing between the two proton configurations in each ^{48}K state. If the shell model overestimates the fraction of $\pi s_{1/2} d_{3/2}^4$ in the final state wavefunction, this may account for the discrepancy in calculated and observed spectroscopic factors. Considering mixed proton configurations further, the two lowest 1^- states manifest from a neutron in $p_{3/2}$ orbital coupled to the $\pi s_{1/2} d_{3/2}^4$ and $\pi s_{1/2}^2 d_{3/2}^3$ configurations, respectively. Both shell-model interactions predict these two configurations to mix substantially, and, indeed, this is what is observed in the current study. It is worth noting that, in a weak coupling model, the two configurations are degenerate, whilst, conversely, mixing pushes them apart in energy. On this point, shell-model calculations predict the first two 1^- states to be separated by less than 1 MeV; from experiment the separation is 1.4 MeV. This implies that the shell model fails to correctly account for the mixing between configurations. Moreover, this accounts for the ground state (which is a 1^-

state) being predicted incorrectly in the models. Interestingly, the situation for the two lowest 2^- states (experimentally, the first two excited states) is in complete contrast, whereby the shell model predicts almost no mixing between the $\pi s_{1/2}d_{3/2}^4$ and $\pi s_{1/2}d_{3/2}^3$ configurations and experiment confirms this, with only the 0.143 MeV excited state being observed. More generally, we note that the overestimation of the spectroscopic factors by the shell model increases according to the percentage of the $\pi s_{1/2}d_{3/2}^4$ configuration in the ^{48}K wavefunction [40]. Additionally, we note that the neutron single-particle energies of $f_{5/2}$, $p_{1/2}$, $p_{3/2}$ and $f_{7/2}$ we extract for ^{48}K (-0.64 , -2.71 , -4.19 and -8.37 MeV) lie in between those of ^{49}Ca (-1.15 , -3.13 , -5.15 and -9.95 MeV) and ^{47}Ar (-0.1 , -2.42 , -3.55 and -8.02 MeV) – cf. Fig 3 in Ref [8].

In summary, we have performed the first measurement of the $^{47}\text{K}(d, p\gamma)^{48}\text{K}$ transfer reaction. Nine new bound excited states have been uniquely identified and spectroscopic factors deduced, providing a benchmark for $\pi(s_{1/2})-\nu(fp)$ interactions in theoretical models. A detailed comparison with state-of-the-art shell-model calculations indicates several key discrepancies between theory and experiment. In particular, the failure of shell-model calculations to predict the 1^- ground state of ^{48}K is traced to incorrect mixing between the proton configurations, evidenced by the energy gap from 1_1^- to 1_2^- (measured here for the first time – see Fig 3). Additionally, neither calculation can account for the existence of the mixed pf -configuration state observed in the current study. Further, an analysis of the spacing and splitting of f - and p -wave orbitals reveals a clear preference for the ‘first-principles’ SDPF-MU interaction over the ‘phenomenological’ SDPF-U interaction. This information is useful for extrapolations to neutron-rich nuclei; for example, calculations for ^{44}P using SDPF-MU indicate $\nu(p_{1/2})-\nu(p_{3/2})$ degeneracy, which is in contrast to SDPF-U predictions. Finally, the experimentally determined spectroscopic factors are found to be systematically smaller than those predicted by theory, which may be due to an overestimation by shell-model calculations of the fraction of $\pi s_{1/2}d_{3/2}^4$ in the final state wavefunctions of levels in ^{48}K . This echoes the difficulty with shell model calculations for neighbouring ^{47}Ar , populated by $^{46}\text{Ar}(d, p)$ [8], indicating that the key limitation in our description of light nuclei around $N=28$ is the poor understanding of the proton component. As such, it is crucial that these nuclei with near-degenerate proton configurations be investigated further in order to benchmark theoretical models in this region of the nuclear chart. Measurements of single-neutron transfer on the $N=28$ nuclei, ^{45}Cl and ^{43}P , using radioactive beams are strongly recommended.

We acknowledge the GANIL facility for provision of heavy-ion beams, and we thank J. Goupil, G. Fremont, L. Ménager, and A. Giret for assistance in us-

ing the G1 beam line and its instrumentation. We acknowledge the AGATA collaboration for the use of the spectrometer. This work was supported by the Science Technology Facilities Council (United Kingdom) under the grants ST/N002636/1, ST/P005314/1 and ST/V001108/1. This work was also partially funded by MICIU MCIN/AEI/10.13039/501100011033, Spain with grants PID2020-118265GB-C42, PRTR-C17.I01, Generalitat Valenciana, Spain with grant CIPROM/2022/54, ASFAE/2022/031, CIAPOS/2021/114 and by the EU NextGenerationEU funds. Additional funding from Spanish grant PID2021-127711NB-I00. This work was partially supported by the U.S. Department of Energy, Office of Science, Office of Nuclear Physics, under contract number DE-AC02-06CH11357. Experimental data and analytical codes can be found at Refs. [47–49]

-
- [1] M. Goeppert Mayer, Phys. Rev. **75**, 1969 (1949).
 - [2] O. Haxel, J. H. D. Jensen, and H. E. Suess, Phys. Rev. **75**, 1766 (1949).
 - [3] B. A. Brown and B. H. Wildenthal, Ann. Rev. Nucl. Part. Sci. **38**, 29 (1988).
 - [4] B. A. Brown, Physics **4**, 525 (2022).
 - [5] D. Steppenbeck *et al.*, Nature **502**, 207 (2013).
 - [6] L. Lalanne *et al.*, Phys. Rev. Lett. **131**, 092501 (2023).
 - [7] O. Sorlin and M.-G. Porquet, Phys. Scr. **2013**, 014003 (2012).
 - [8] L. Gaudefroy *et al.*, Phys. Rev. Lett. **97**, 092501 (2006).
 - [9] A. Signoracci and B. A. Brown, Phys. Rev. Lett. **99**, 099201 (2007).
 - [10] L. Gaudefroy *et al.*, Phys. Rev. Lett. **99**, 099202 (2007).
 - [11] D. Mengoni *et al.*, Phys. Rev. C **82**, 024308 (2010).
 - [12] S. Calinescu *et al.*, Phys. Rev. C **93**, 044333 (2016).
 - [13] K. Nowak *et al.*, Phys. Rev. C **93**, 044335 (2016).
 - [14] K. Kreim *et al.*, Physics Letters B **731**, 97 (2014).
 - [15] J. Papuga *et al.*, Phys. Rev. C **90**, 034321 (2014).
 - [16] W. Królas *et al.*, Phys. Rev. C **84**, 064301 (2011).
 - [17] T. Burrows, Nuclear Data Sheets **108**, 923 (2007).
 - [18] J. Chen, Nucl. Data Sheets **179**, 1 (2022).
 - [19] M. Assié *et al.*, Nucl. Instrum. Meth. A **1014**, 165743 (2021).
 - [20] S. Akkoyun *et al.*, Nucl. Instrum. Meth. A **668**, 26 (2012).
 - [21] E. Clément *et al.*, Nucl. Instrum. Meth. A **855**, 1 (2017).
 - [22] M. Assié, J. Phys. Conf. Ser **1643**, 012070 (2020).
 - [23] M. Rejmund *et al.*, Nucl. Instrum. Meth. A **646**, 184 (2011).
 - [24] P. Chauveau *et al.*, Nucl. Instrum. Meth. B **541**, 61 (2023).
 - [25] O. Stężowski *et al.*, Eur. Phys. J. A **59**, 118 (2023).
 - [26] A. J. Boston *et al.*, Eur. Phys. J. A **59**, 213 (2023).
 - [27] F. C. L. Crespi, J. Ljungvall, A. Lopez-Martens, and C. Michelagnoli, Eur. Phys. J. A **59**, 111 (2023).
 - [28] A. Lopez-Martens *et al.*, Nucl. Instrum. Meth. A **533**, 454 (2004).
 - [29] S. Ottini-Hustache *et al.*, Nucl. Instrum. Meth. A **431**, 476 (1999).
 - [30] E. Farnea *et al.*, Nucl. Instrum. Meth. A **621**, 331 (2010).
 - [31] I. J. Thompson, “Fresco v3.1.1,” www.fresco.org.uk.

- [32] W. W. Daehnick, J. D. Childs, and Z. Vrcelj, Phys. Rev. C **21**, 2253 (1980).
- [33] P. D. Kunz, “DWUCK4,” (Available at www.oecd-neutron.org/tools/abstract/detail/nesc9872).
- [34] A. Matta *et al.*, J. Phys. G **43**, 045113 (2016).
- [35] S. Agostinelli *et al.*, Nucl. Instrum. Meth. A **506**, 250 (2003).
- [36] J. Tostevin, “University of Surrey version of the code TWOFNR (of M. Toyama, M. Igarashi and N. Kishida) and code FRONT (private communication). v20,” .
- [37] A. Koning and J. Delaroche, Nucl. Phys. A **713**, 231 (2003).
- [38] R. C. Johnson and P. C. Tandy, Nucl. Phys. A **235**, 56 (1974).
- [39] R. C. Johnson and P. J. R. Soper, Phys. Rev. C **1**, 976 (1970).
- [40] C. J. Paxman, Ph.D. thesis, University of Surrey (2024).
- [41] J. Lee, M. B. Tsang, and W. G. Lynch, Phys. Rev. C **75**, 064320 (2007).
- [42] A. Matta *et al.*, Phys. Rev. C **99**, 044320 (2019).
- [43] B. A. Brown and W. D. M. Rae, Nucl. Data Sheets **120**, 115 (2014).
- [44] F. Nowacki and A. Poves, Phys. Rev. C **79**, 014310 (2009).
- [45] T. Otsuka *et al.*, Phys. Rev. Lett. **104**, 012501 (2010).
- [46] Y. Utsuno *et al.*, Phys. Rev. C **86**, 051301 (2012).
- [47] W. N. Catford *et al.*, (2021), 10.26143/GANIL-2021-E793S_19.
- [48] A. Matta *et al.*, (2024), 10.5281/zenodo.13748333.
- [49] C. J. Paxman *et al.*, (2024), 10.5281/zenodo.13748642.